Electronic Supplementary Material (ESI) for Green Chemistry.

Supporting Information

Decarboxylative [4+2] Cycloaddition via Ligand-to-Metal Charge Transfer Photoexcitation of Cu-MOF

Wenjing Wang[a,b], Di Zeng[a,b], Juxue Wang[a,b], Bingkun Cui[a,b], Taikang Jia[a,b], Ruofan Li[a,b], Hongxiang Chu[a,c], Yu Zhang[a,b], Ling Zhang[a,b] and Wenzhong Wang[a,b,c]**

[a] State Key Laboratory of High Performance Ceramics and Superfine Microstructure, Shanghai Institute of Ceramics, Chinese Academy of Sciences, 1295 Dingxi Road, Shanghai, 200050, People's Republic of China

[b] Center of Materials Science and Optoelectronics Engineering, University of Chinese Academy of Sciences, Beijing, 100049, People's Republic of China

[c] School of Chemistry and Materials Science, Hangzhou Institute for Advanced Study, University of Chinese Academy of Sciences, 310024, People's Republic of China

* Email for corresponding author: lingzhang@mail.sic.ac.cn; wzwang@mail.sic.ac.cn

Experimental Section

Materials

All reagents were purchased from chemical companies without secondary purification.

$Cu(NO_3)_3 \cdot 3H_2O$ (>98%), ethanol, and trimesic acid were purchased from Sinopharm Chemical Reagent Co., Ltd. $H_3O_{40}PW_{12} \cdot xH_2O$ were purchased from Shanghai Macklin Biochemical Technology Co., Ltd. All the other organic reagents were purchased from Adamas-beta LTD.

Photocatalyst preparation

PW@HKUST-1. 1.0 g $Cu(NO_3)_2 \cdot 3H_2O$, 0.92 g trimesic acid and 1.2 g $H_3[PW_{12}O_{40}]$ were fully dissolved in 200 mL ethanol. The solution was continuously stirred for 24 hours at room temperature until precipitates appeared. The collected precipitate was washed several times with ethanol.

Characterization

Powder X-Ray diffraction (PXRD) patterns were collected on the Rigaku 2550V X-ray diffractometer with Cu Kα radiation. Morphology and microstructure of the PW@HKUST-1 were investigated upon a Hitachi SU-8220 field emission scanning electron microscope (SEM) under a 10 kV accelerating voltage. Thermogravimetric analysis (TGA) was obtained under flowing Ar on an SDT Q600 V8.3 Build 101 thermal analysis device with a temperature-increasing rate of 5 ^{o}C /min in Ar. N_2 sorption experiments were performed on a Micromeritics ASAP2460 aperture analyzer. The inductively coupled plasma optical emission spectroscopy (ICP-OES, Agilent 5110) was used to determine the PW. Electron paramagnetic resonance (EPR) spectra were obtained from a Bruker EMXnano EPR spectrometer (9.828 GHz, X-band). UV-visible (UV-vis) absorption spectra were measured using a Hitachi U-3010 spectrophotometer. Photoluminescence (PL) spectra were performed using Hitachi F-4600 fluorescence spectrophotometer. The X-ray photoelectron spectroscopy (XPS) valence spectra were measured at a Thermo Fisher ESCALAB 250Xi XPS microprobe with Al Kα radiation (1253.6 eV). The binding energies were calibrated by the C 1s peak at 284.8 eV.

Electrochemical analysis

Electrochemical analyses were conducted on a Chenhua CHI 660D electrochemical workstation with conventional three-electrode quartz cell system. Typically, a platinum sheet and a saturated calomel electrode (SCE) were used as the counter and reference electrodes, respectively, and the as-prepared photocatalysts were coated on fluorine-doped tin oxide (FTO) glass and functioned as working electrodes. Photocurrent spectra were performed in 0.1 M sodium sulfate.

Synthesis of p-xylene from furan derivatives with acrylic acid over the catalysts

Typically, 2.5 mmol 2,5-dimethylfuran (DMF) and 15 mmol acrylic acid (AA) were added into a quartz bottle with a given mass of catalysts, n-heptane as an internal standard, and the experiment was performed with 400 nm LED (36 W) for 3 h in CO_2 atmosphere. After the reaction, the liquid products were analyzed using Gas Chromatography (GC). The GC 2060 with a SE-54 column and a flame ionization detector (FID) was used to analyze the yields and selectivity of liquid products. The Tianmei 7900 with with a TDX-01 column and thermal conductivity detector (TCD) was used to analyze the yields and selectivity of gaseous products.

Quantitative calculation

$$\text{Conversion of DMF} = \frac{\text{moles of DMF reacted}}{\text{initial moles of DMF}} \times 100\ \%$$

$$\text{Selectivity of product} = \frac{\text{moles of product}}{\text{moles of DMF reacted}} \times 100\ \%$$

$$\text{Yield} = \text{Conversion} \times \text{Selectivity}$$

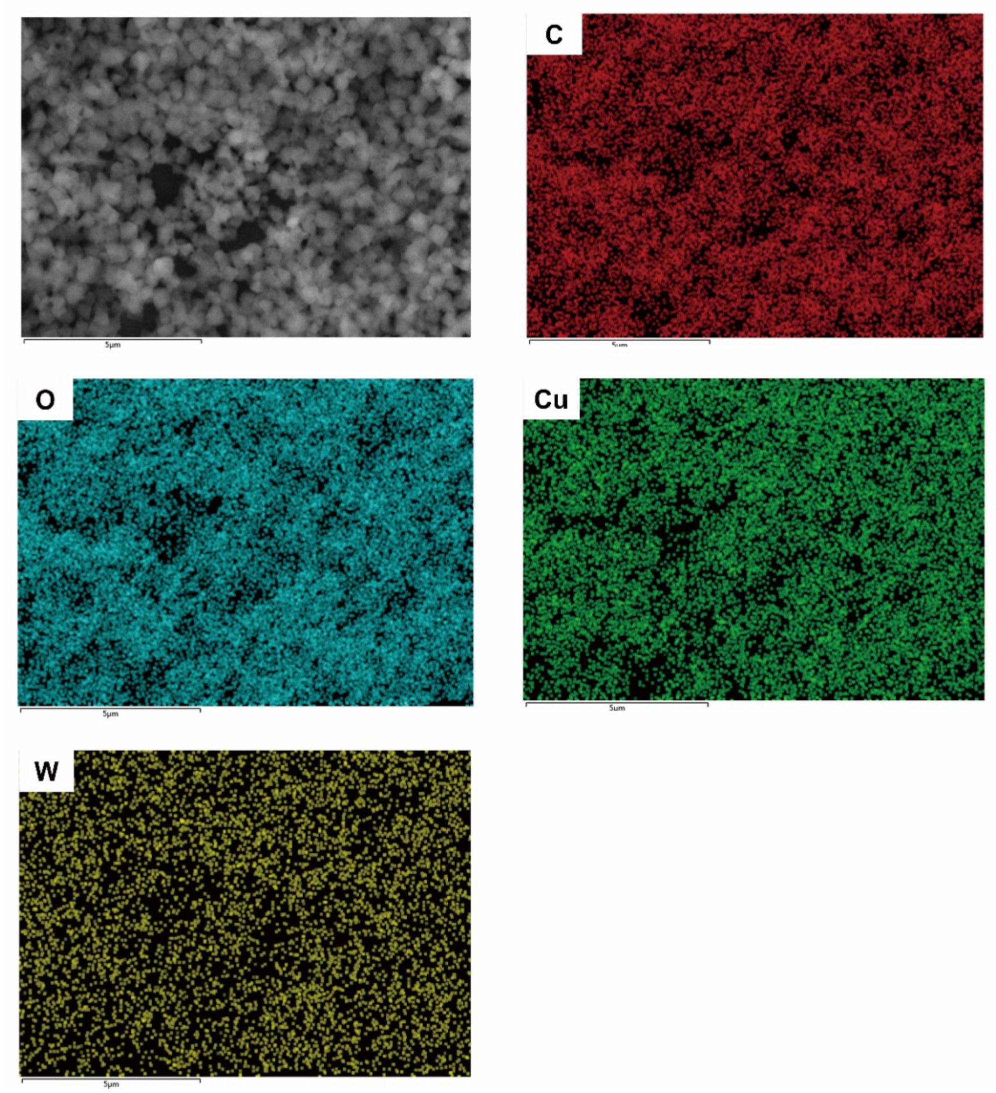

Figure S1. Elemental distribution under SEM scan by energy dispersion spectra (EDS). Red: C, blue: O, green: Cu, yellow: W.

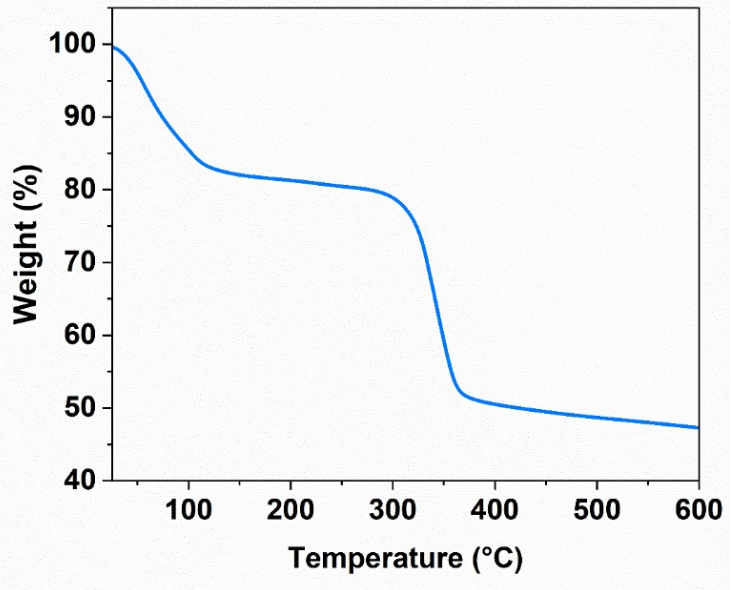

Figure S2. TGA analysis of PW@HKUST-1.

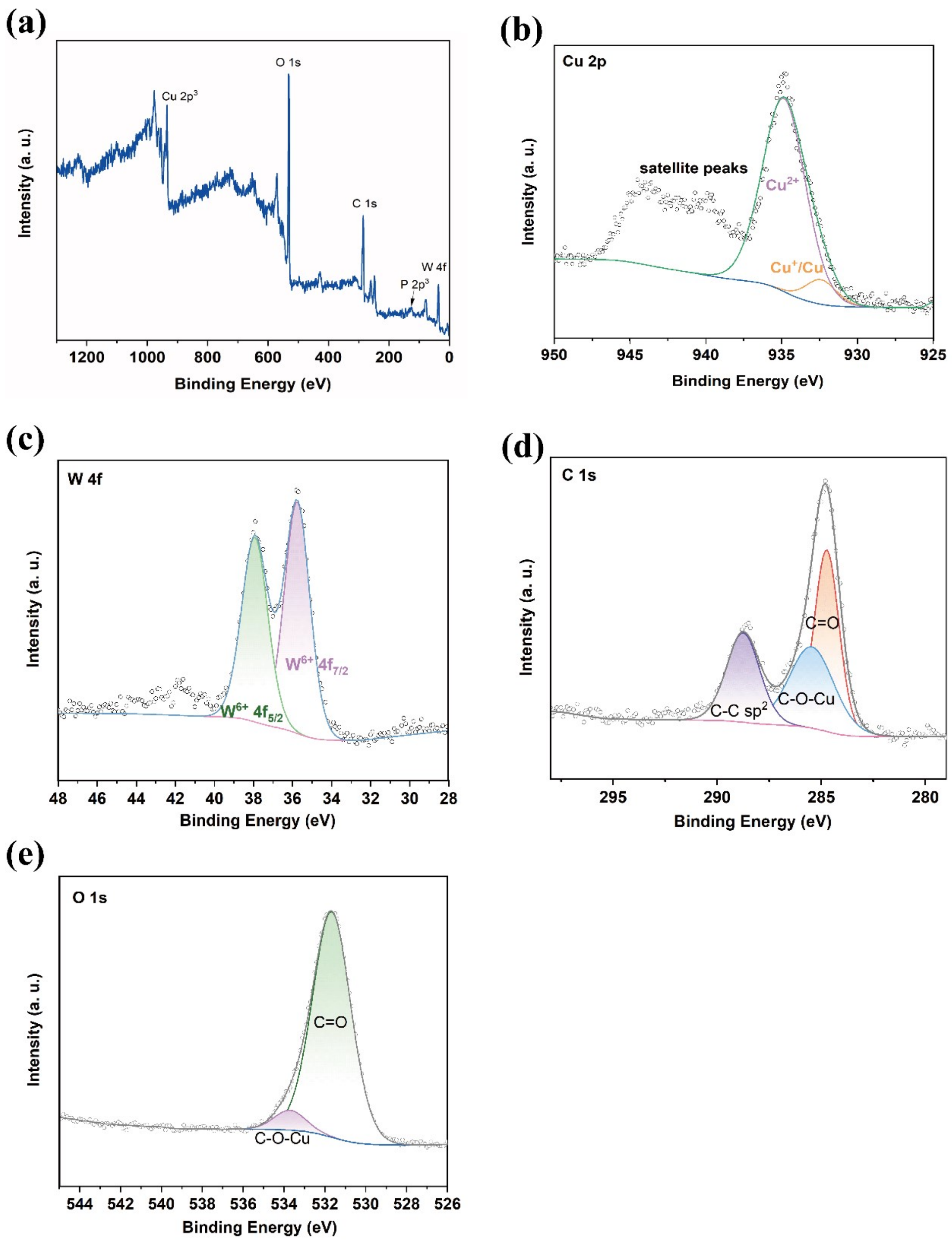

Figure S3. XPS spectra of PW@HKUST-1, (a) survey spectrum, (b) Cu 2p, (c) W 4f, (d) C 1s, (e) O 1s

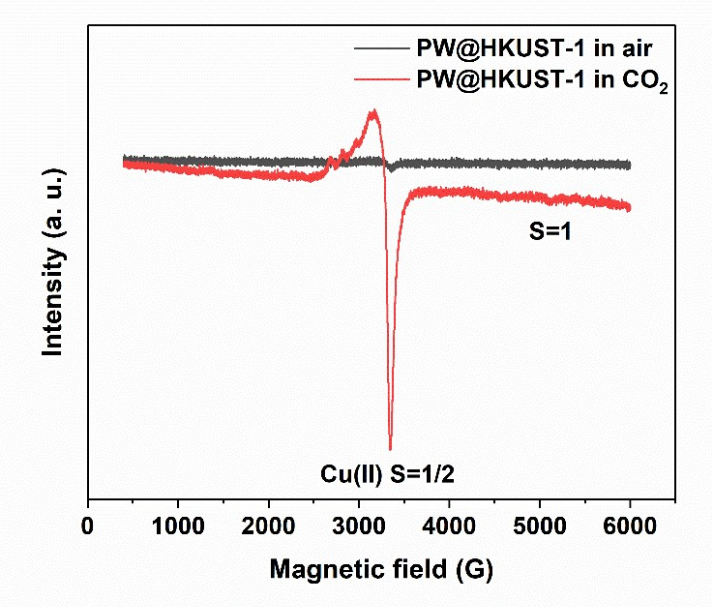

Figure S4. X-band EPR spectra of PW@HKUST-1 in different atmospheres at room temperature.

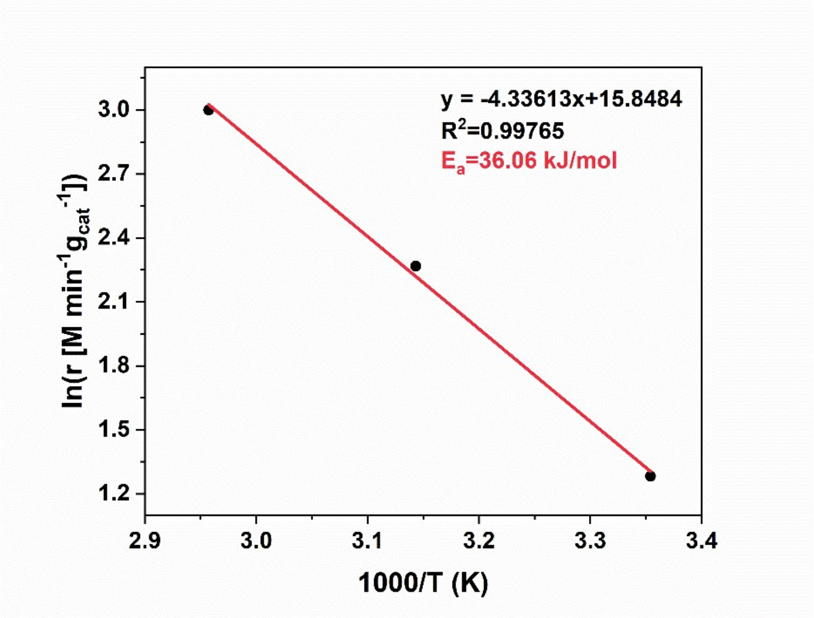

Figure S5. Arrhenius plot with calculated activation energy.

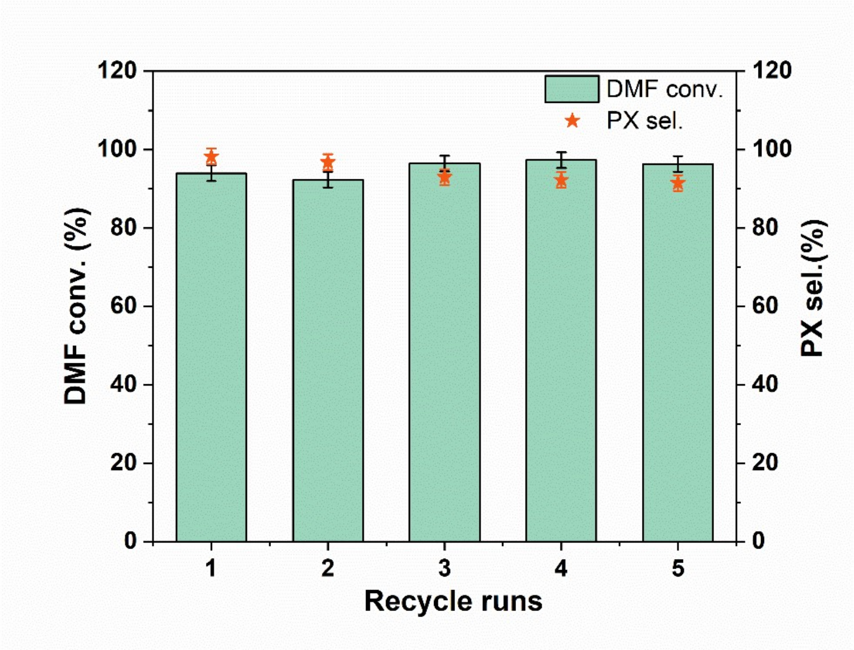

Figure S6. The cycle performance of PW@HKUST-1.

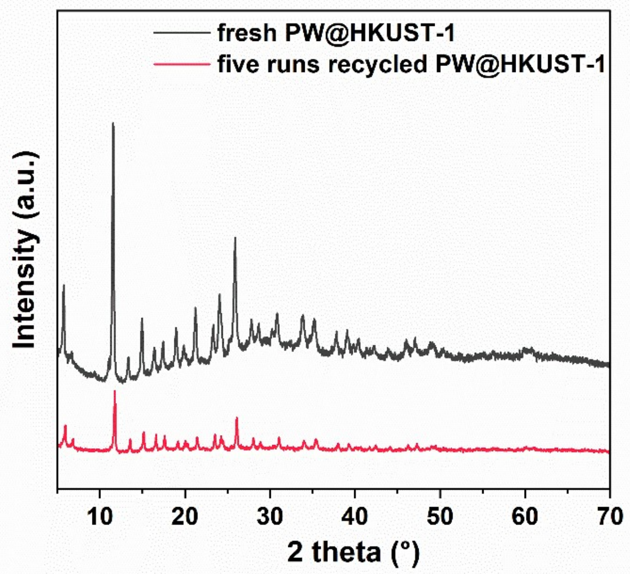

Figure S7. XRD patterns of fresh and used PW@HKUST-1.

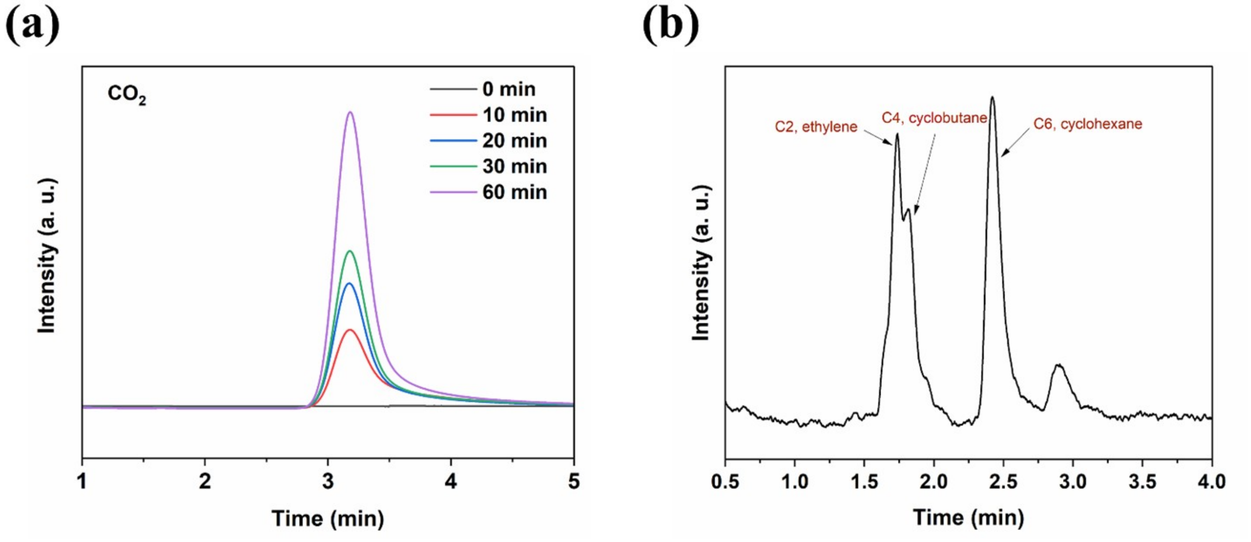

Figure S8. The AA decarboxylated products by gas chromatography (a) signal of CO$_2$, Tianmei 7900 with a TDX-01 column and TCD (b) signal of hydrocarbon, Tianmei 7900 with a SE-54 column and FID.

It is proposed that deprotonation of carboxyl groups occurs in POM sites, which was considered as a proton acceptor (soft basicity) due to the presence of metal terminal oxygen (W=O).[1]

The proton dissociated from the carboxyl groups (AA) transferred to the POM. The change in absorbance of the PW@HKUST-1 before and after reaction was characterized using UV-vis absorption spectroscopy. The absorption intensity of the reacted catalyst is significantly enhanced in 400-800 nm range (**Figure S9**), which is the absorption band of low-valent tungsten in PW[2, 3] due to the storage of protons and electrons. When the reaction starts, the oxa-norbornene anion will take the proton away from PW, completing the cycle reaction of the proton, as we proposed in **Scheme 2**.

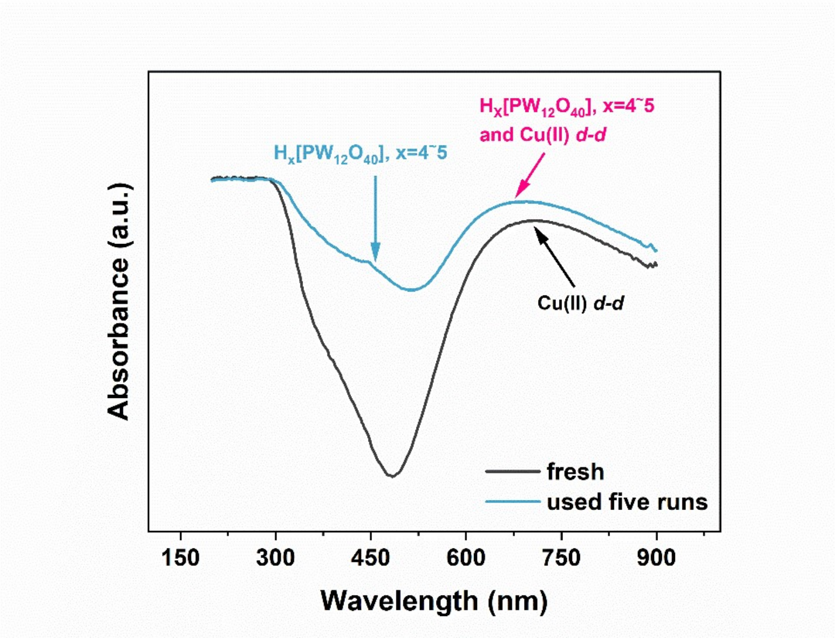

Figure S9. UV-vis absorption spectra of fresh and used PW@HKUST-1.

Table S1. The specific data of the pore canal of the samples.

	Surface Area ($m^2 \cdot g^{-1}$)	**Pore Volume ($cm^3 \cdot g^{-1}$)**	**Pore Size (nm)**
PW@HKUST-1	624.1	0.38	9.9

Table S2. The composition of catalysts calculated from ICP-OES.

	Cu (wt %)	**W (wt %)**
PW@HKUST-1	25.1	14.4

Table S3. PX yield with various molar ratio of AA/DMF.

Entry	**Molar ratio**	**Conv. [%]**	**PX Sel. [%]**	**PX yield [%]**
1	1:1	38.7	47.0	18.2
2	3:1	64.8	52.9	34.3
3	6:1	94.4	92.6	98.1
4	9:1	89.3	28.8	25.7

Catalyst	**Dienophile**	**Activation energy (kJ mol^{-1})**	**Ref.**
H-Beta, Sn-BEA and Zr-BEA zeolite	ethylene	50-68	4
$Nb_2O_5/NbOPO_4$	ethylene	37.7	5
Nb/MCM	ethylene	47.7	6
Nb/SiO_2	ethylene	73.6	
K/Rb/Cs doped HPW	ethylene	57.9	7
SnPO-1.50	ethylene	61.1	8
HUSY-12 zeolite (Si/Al=6)	ethanol	55.8	9
Bi-BTC	acrylic acid	47.4	10
[Bmim]HSO_4/Cu_2O/4,7-diphenyl-1,10-phenanthroline	acrylic acid	64.8	11
PW@HKUST-1	acrylic acid	36.1	*This work*

Table S4. Summary of the references on activation energy of the conventional thermal catalysts.

Table S5. Scope of reaction with different dienes.

Reactant	**Conversion (%)**	**Aromatic products**	**Yield (%)**
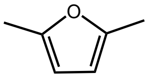	94.4	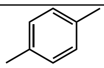	92.6
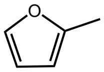	99.9	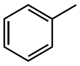	82.7
	trace		trace
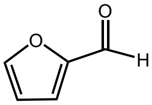	trace	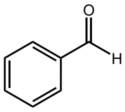	trace

Reaction condition: 2.5 mmol dienes, 15 mmol AA, 25 ^{o}C, 3 h, 1 bar CO_2, 200 mg catalyst, irradiation with 400 nm LED.

Table S6. Summary of articles about DMF and AA to PX conversion.

Catalyst	**Additive**	**T (^{o}C)**	**P (bar)**	**Time (h)**	**DMF Conv. (%)**	**PX Yield (%)**	**Ref.**
Beta (Si/Al=150)	-	200	30	0.168	100	83	12
[Bmim]HSO_4/ Cu_2O/4,7-diphenyl-1,10-phenanthroline	1-methyl-2-pyrrolidinone/quinoline	25/210	1	1+4	87	72.2	13
$Sc(OTf)_3$+H_3PO_4/Cu_2O/ 4,7-diphenyl-1,10-phenanthroline	1-methyl-2-pyrrolidinone/quinoline	15/210	1	1+4	90	56.7	14
Bi-BTC	acetone	160	10	24	99	92	15
PW@HKUST-1	-	25	1	3	94	92.6	This work

References:

1. S. Wang and G. Yang, *Chem. Rev.*, 2015, **115**, 4893-4962.
2. B. Rausch, M. D. Symes, G. Chisholm and L. Cronin, *Science.*, 2014, **345**, 1326-1330.
3. J. Chen, L. Vilà-Nadal, A. Solé-Daura, G. Chisholm, T. Minato, C. Busche, T. Zhao, B. Kandasamy, A. Y. Ganin, R. M. Smith, I. Colliard, J. J. Carbó, J. M. Poblet, M. Nyman and L. Cronin, *J. Am. Chem. Soc*, 2022, **144**, 8951-8960.
4. J. Yu, S. Zhu, P. J. Dauenhauer, H. J. Cho, W. Fan, R. J. Gorte and F. R. C. E. Energy, *Catal. Sci. Technol.*, 2016, **6**, 5729-5736.
5. J. Yin, C. Shen, X. Feng, K. Ji and L. Du, *ACS Sustain. Chem. Eng.*, 2018, **6**, 1891-1899.
6. Y. Zhao, K. Wang, Z. Sun, Q. Zhang, Z. Wang, Y. Liu, H. He and Y. Cao, *Green Chem.*, 2022, **24**, 4095-4107.
7. C. Wu, Z. Yang, J. Li, C. Liu and W. Dong, *Sustain. Energy Fuels.*, 2022, **6**, 4458-4469.
8. X. Feng, Z. Cui, K. Ji, C. Shen and T. Tan, *Appl. Catal. B.*, 2019, **259**, 118108.
9. I. F. Teixeira, B. T. W. Lo, P. Kostetskyy, M. Stamatakis, L. Ye, C. C. Tang, G. Mpourmpakis and S. C. E. Tsang, *Angew. Chem. Int. Ed.,* 2016, **128**, 13255-13260.
10. J. Y. Yeh, S. S. Chen, S. C. Li, C. H. Chen, T. Shishido, D. C. W. Tsang, Y. Yamauchi, Y. P. Li and K. C. W. Wu, *Angew. Chem. Int. Ed.*, 2021, **60**, 624-629.
11. L. Ni, J. Xin, K. Jiang, L. Chen, D. Yan, X. Lu and S. Zhang, *ACS Sustain. Chem. Eng.*, 2018, **6**, 2541-2551.
12. J. A. Mendoza Mesa, F. Brandi, I. Shekova, M. Antonietti and M. Al-Naji, *Green Chem.*, 2020, **22**, 7398-7405.
13. L. Ni, J. Xin, K. Jiang, L. Chen, D. Yan, X. Lu and S. Zhang, *ACS Sustain. Chem. Eng.*, 2018, **6**, 2541-2551.
14. L. Ni, J. Xin, H. Dong, X. Lu, X. Liu and S. Zhang, *ChemSusChem.*, 2017, **10**, 2394-2401.
15. J. Yeh, S. S. Chen, S. Li, C. H. Chen, T. Shishido, D. C. W. Tsang, Y. Yamauchi, Y. Li and K. C. W. Wu, *Angew. Chem. Int. Ed.*, 2021, **60**, 624-629.